RSC Advances




ROYAL SOCIETY OF CHEMISTRY

www.rsc.org/advances

Page 1 of 8 RSC Advances

RSC Advances RSC Publishing

ARTICLE

# Facile Synthesis of Magnetic Resorcinol–Formaldehyde (RF) Coated Carbon Nanotubes for Methylene blue removal

Received 00th January 20xx,
Accepted 00th January 20xx

DOI: 10.1039/x0xx00000x

www.rsc.org/

Dianqiu Zheng†, Min Zhang* †, Lei Ding†, Yanwei Zhang†, Jing Zheng†, Jingli Xu*,†

In this paper, magnetic resorcinol–formaldehyde (RF) resin coated carbon nanotubes were synthesized from hydrophilic magnetic carbon nanotubes (CNTs) with the extended stober method. Firstly, magnetic CNTs composites (CNTs@$Fe_3O_4$) were synthesized by the high temperature decomposition process using the iron acetylacetonate as raw materials. Then the resorcinol–formaldehyde polymer can be easily coated on the magnetic CNTs with the extended stober method Finally, numerous of gold nanoparticles were assembled on the surface of CNTs@$Fe_3O_4$@RF by reducing $Au^{3+}$ between the RF shell and $HAuCl_4$ solution; meanwhile, the mesoporous carbon coated CNTs@$Fe_3O_4$ can also be obtained by calcinations of the CNTs@$Fe_3O_4$@RF composites in nitrogen atmosphere. The resulting CNTs@$Fe_3O_4$@RF@Au or CNTs@$Fe_3O_4$@C composites show not only a magnetic response to an externally applied magnetic field, but also can be a kind of catalyst or adsorbent to catalyze or adsorb the methylene blue (MB), in the ambient temperature.

## Introduction

Recently, the surface functionalization of CNTs with various inorganic nanoparticles(NPs) such as metals, metal oxides and semiconducting nanoparticles has aroused great interest due to their unique functionalities in the CNTs and inorganic nanoparticles, making these materials applicable in catalysis, gas sensors, fuel cell, supercapacitor, and environmental treatments etc[1-9]. However, the poor solubility of CNTs in different solvents has imposed great limitations to above mentioned applications. The strategies pretreated by the high concentrated acid can effectively solve the insolubility of the CNTs, but it causes the serious environmental pollution and destroys the structure of the CNTs. Therefore it has been highly desired to functionalize CNTs with various inorganic NPs to be dispersible and easily separable without destruction of their structure by a mild method. In view on these, the polyol-assisted synthesis of NPs as a highly attractive way has been proposed to functionalize CNTs with metal-oxide NPs[10]. The proposed process would exhibit the following attractive features: (1) The CNTs will not be pretreated by high concentrated acid or doping with heteroatoms, which will greatly simplify the procedures and reduce the negative impact on the environments. (2) By using this process, the metal oxide NPs decorated on the CNT will be highly functionalized with abundant hydroxylic groups, which can be further modified due to the abundance of hydroxyl groups. This will greatly improve the applications of the multifunctional composites. One the other hand, decorating CNTs with magnetic nanoparticles has been been emerging to be an interesting area of advanced research owing to their potential applications in magnetic data storage, determination of microorganisms, magnetic resonance imaging, electrochemical biosensor and magnetically guided drug delivery systems [11–13]. To apply magnetic CNTs in the above applications, more works have been done to functionalize magnetic CNTs surface with another phase to enhance compatibility and functionality.

Resorcinol-formaldehyde (RF) resin, glucose and polydopamine have been used to functionalize the nanomaterials due to the attractive properties of such as low cost, high surface areas, remarkable electrical conductivity, and outstanding thermal and mechanical properties[14-17]. Among these materials, RF resin, a three-dimensional networks structured polymer is highly desired. Since Qiao group have successfully extended the classical Stöber method to conveniently synthesize monodisperse RF resin polymer colloidal spheres and then carbon spheres by the carbonization of the RF resin spheres[18], the RF-Stöber method has been widely used to make core-shell nanoparticles because of the simple setup and excellent reproduciblility[19-24]. Besides the above mentioned, RF resin is known to reduce metal salts within a solution into metal nanoparticles via the hydroxyl functional groups. A range of metals, including Ag, Au, Pd have been successfully reduced and surface modified by the deposited RF resin without the need for the addition of a reducing agent[25-28]. Then, the growing numbers of applications of cores@RF composites have driven us to further extend the Stöber method to synthesize RF resin coated magnetic CNTs with well defined core-shell structures.

Herein, we describe the synthesis of magnetic CNTs@RF nanocables by an extended Stöber method for the first time. Subsequent annealing of the magnetic CNTs@RF nanocables to carbonize the RF shell results in unique core–shell structured mesoporous magnetic CNTs@carbon nanocables; Meanwhile, numerous of gold nanoparticles were assembled on the surface of CNTs@$Fe_3O_4$@RF by reducing $Au^{3+}$ between the CNTs@$Fe_3O_4$@RF solid and $HAuCl_4$ solution, seen in Scheme 1.

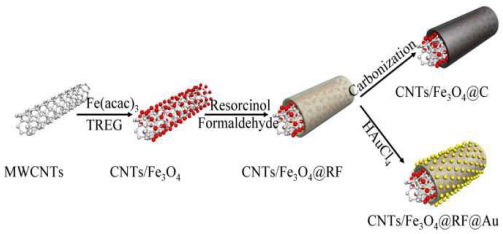


**Scheme 1** Synthesis of core–shell structured magnetic CNTs@RF nanocables

## Experimental Section

### Chemicals

Multiwalled CNTs (MWCNTs) with a mean diameter of 60–100 nm and length >5 um were provided by the Shenzhen Nanotech Port Co. Ltd. Methylene blue (MB), sodium borohydride were purchased from Shanghai Lanji Co. Ltd. (Shanghai, China). Chloroauric acid, triethylene glycol(TREG, 99%) were obtained from Aldrich. Deionized water was prepared with a Milli-Q water purification system (Millipore, Milford, MA). Iron(III) acetylacetonate ($Fe(acac)_3$, 99%) was purchased from Acros. Resorcinol, formaldehyde solution, ammonia solution (28–30%), cetyl trimethylammonium bromide (CTAB) were purchased from shanghai chemical reagent company. Other reagents were of analytical grade or better and used without further purification.

### Synthesis of CNTs@$Fe_3O_4$ nanocomposites

CNTs@$Fe_3O_4$ nanocomposites with high saturation magnetization were synthesized according to previous work with some modification[13]. Firstly, 400 mg $Fe(acac)_3$ (99%, Alfa) and 100 mg MWCNTs were added to 60 mL TREG and ultrasonicated for 10 minutes. The resulting mixture was then heated to 278 °C under argon protection and kept at reflux for 30 min. After cooling to room temperature, the obtained nanocomposites were magnetically separated by a magnet and washed with ethanol for several times and dried at 60 °C in vacuum oven.

### Synthesis of CNTs@$Fe_3O_4$@RF core–shell structures

The core–shell CNTs@$Fe_3O_4$@RF nanostructures were prepared by a surfactant-assistant sol–gel (Stöber method) coating method. Briefly, 100 mg of the as-prepared CNTs@$Fe_3O_4$ nanocomposites were homogeneously dispersed in the mixture of 60 mL deionized water and 25 mL ethanol by ultrasonication for 15 minutes. Followed by the addition of 150 mg CTAB, the mixed solution was homogenized for 30 min to form a uniform dispersion. Next, 64 mg resorcinol and 70 μL formaldehyde were added to the dispersion with continuous ultrasonication for 10 min. After the addition of 0.4 mL ammonia solution, the final mixture was stirred at room temperature (25 ℃) for 20 h. The product was collected *via* a magnet and washed with deionized water and ethanol for 3 times to remove by-products, followed by dried in vacuum at 60℃ overnight.

### Synthesis of CNTs@$Fe_3O_4$@C and CNTs@$Fe_3O_4$@RF-Au composites

The mesoporous CNTs@$Fe_3O_4$@C composites was obtained by the carbonization of core–shell structured RF resin nanocomposites under a $N_2$ atmosphere at 150 ℃ for 1 h with a heating rate of 3 ℃ /min, which was followed by further treatment at 500 ℃ for 5 h with a heating rate of 1 ℃ /min; The CNTs@$Fe_3O_4$@RF-Au was synthesized as follows: 40 mg of the CNTs/$Fe_3O_4$@PFR composite solution was added to 30 mL water by sonication to form a stable dispersion, then, 5 mL $HAuCl_4$(1 mg/mL) was added into the flask and heated at 80 ℃ for 1 h. The product was collected and washed by water and ethanol several times and dried for further use.

### Instrumentation

The SEM images were obtained by a SS-550 scanning electron microscope (Shimadzu, Japan). Fourier transform infrared (FT-IR) spectra (4000-400 $cm^{-1}$) in KBr were recorded using the AVATAR 360 FT-IR spectrophotometer (Nicolet, Waltham, USA). The data of UV-vis adsorption were obtained by using UV-2450 spectrophotometer (Shimadzu, Japan). The crystal structure of nanoparticles was determined by X-ray diffractometer (XRD). The XRD pattern of each sample was recorded with a Shimadzu (Japan) D/Max-2500 diffractometer, using a monochromatized X-ray beam with nickel-filtered Cu Kα radiation. The XRD patterns were collected in the range of $5°<2\theta<80°$ with a dwelling time of 2s and a scan rate of 6.0°/min. The substance is automatically searched by using JCPDS-International Center for Diffraction Data. The X-ray photoelectron spectrometeric(XPS) spectra were obtained on a Shimadzu (Japan) Kratos AXIS Ultra DLD X-ray photoelectron spectrometer with an Mg Kα anode (15kV, 400W) at a takeoff angle of 45°. The source X-ray was not filtered, and the instrument was calibrated against the C1s band at 285eV. The size and morphology of the nanoparticles were measured by a FEI (Netherlands) Tecnai-20 Transmission Electron Microscopy. Magnetic properties were measured with a LDJ9600-1 (U.S. A.) vibrating sample magnetometer at room temperature. $N_2$ adsorption-desorption isotherms were determined on a Micromeritics ASAP 2460 at 77K, from which the surface area($S_{BET}$), pore volume($V_p$) and pore diameter($D_p$) were calculated by applying Brunauer-Emmett-Teller (BET) and Barrett-Joyner-Halenda(BJH) models to the desorption branches.

### Catalytic Properties of the CNTs@$Fe_3O_4$@RF@Au Nanocables

The reduction of MB by $NaBH_4$ was chosen as a model reaction for the efficiency testing of the Au-immobilized nanoparticle. A given amount of the magnetic catalysts were added into a solution with MB (20 mL, $2\times10^{-4}$ mol/L), in which the volume of the mixture was adjusted to 40 mL with $H_2O$. After that, an aqueous solution of $NaBH_4$ (1 mL, 0.4 mol/L) was rapidly injected at room temperature with stirring. The colour of the mixture gradually vanished, indicating the reduction of the MB dye. Changes in the concentration

RSC Advances



of MB were monitored by examining the variations in the maximal UV-Vis absorption at 665 nm. After the catalytic reaction was completed, the nanocatalysts were separated by externally applied magnetic field and then repeated for the catalytic reaction. The recyclability of the nanoparticle catalysis was determined by measuring the maximal UV-Vis absorption of MB at the end of each catalytic degradation reaction.

## Results and Discussion

### RF resin Coated Magnetic CNTs

The synthetic procedures for core–shell structured magnetic CNTs@RF are illustrated in scheme 1. Firstly, $Fe_3O_4$ particles were successfully coated on the CNTs. The representative TEM and FSEM images of the as-synthesized magnetic CNTs are shown in Fig. 1(a-b), Fig. S1a. The $Fe_3O_4$ particles are uniformly decorated on the surface of the CNTs and the average size is of around 8 nm. As followed, the resorcinol and formaldehyde were coated on the magnetic CNTs, which were obtained at room temperature by an extended Stöber method involving base catalytic co-assembly of RF/CTAB and deposition of RF resin. According to the TEM and SEM images (Fig. 1(c-d), Fig. S1b), the well-defined CNTs@$Fe_3O_4$ @RF tri-layer structure is formed. All the CNTs@$Fe_3O_4$ composites are wrapped by the RF resin coating layer and the thickness of RF shell is of about 5-10 nm. This synthetic approach is highly reproducible and allows facile control over the size of the RF shell thickness. As seen in Fig. 1(e-j), the thickness of the as-prepared RF shell could be tailored from 10 nm to 50 nm by increasing the amount of R and F while keeping the other synthetic parameters constant. No obvious changes in size or shape of the $Fe_3O_4$ cores are observed after loading of the RF resin. When the concentration of resorcinol exceeded, a complete shell can be obtained, but RF spheres also appeared on the shell surface as a result of homogeneous nucleation( Fig. 1(i-j)).

To further understand the formation process of RF coating on hydrophilic magnetic carbon nanotube, we conducted a set of experiments to evaluate the influence on the RF coating by using the hydrophobic carbon nanotubes and hydrophilic carbon nanotubes. As shown in the TEM images(Fig. S2), the uniform RF can be well coated on the hydrophilic carbon nanotube. While as for the hydrophobic carbon nanotube, the severe aggregation was observed in the reaction vessel(data not shown). This fully indicates that the successfule RF coating on the CNTs was attributed to the hydrophilic property of CNTs. While in our work, triethylene glycol (TREG) was selected as solvent and a reducing agent in this synthesis, which endows the magnetic carbon nanotube stabilizing with a layer of hydrophilic polyol molecules and thus good water-dispersibility. And it is expected that the RF can be well coated on the magnetic carbon nanotubes, the mechanism of coating is also in accordance with others' work[14,15].

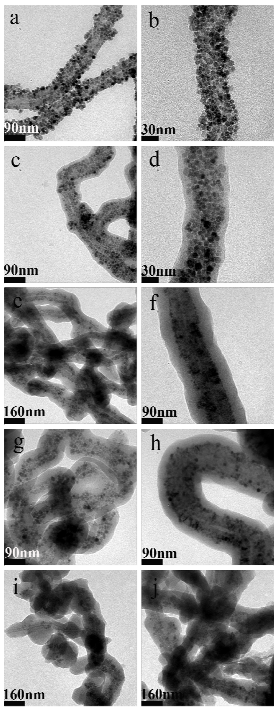


**Fig. 1** TEM images of as-synthesized nanocables: (a-b) CNTs@$Fe_3O_4$ and (c-j) CNTs@$Fe_3O_4$ @RF(R=32 mg, F=35 uL c,d; R=64 mg, F=70 uL e,f; R=128 mg, F=70 uL g,h; R=256 mg, F=140 uL i,j;)

### Mesoporous carbon coated CNTs@$Fe_3O_4$

The RF resin coating was found to be an extremely versatile platform for secondary reaction, leading to tailoring of coating for diverse functional uses. The RF coated magnetic CNTs could be easily transformed into magnetic CNTs@carbon (CNTs@$Fe_3O_4$ @C) core-shell nanocables through the calcinations of as-prepared CNTs@$Fe_3O_4$ @RF precursors at 500℃ under $N_2$ atmosphere for 5 hours. From the TEM images (Fig. 2(a-b)), we can see that the CNTs@$Fe_3O_4$ @C nanocables have uniform shell thicknesses (ca. 20 nm). Compared to the CNTs@$Fe_3O_4$ @RF precursors (Fig. 1(e-f)), the thicknesses of the carbon shells and the diameters of the magnetic CNTs core were reduced, resulting from the shrinkage of RF.

In the case of synthesis of Au NPs, the RF resin and its derivatives can act as reactive templates, which will facilitate the synthetic procedures for polymer-supported gold NPs within one pot step. Due to the hydroxyl-rich groups of the outer RF shell, $AuCl^{4-}$ can be reduced into Au NPs on the shell surface without the use of other reducing agents or surfactants by reducing $Au^{3+}$ between the CNTs@$Fe_3O_4$ @RF solid and $HAuCl_4$ solution. It means that the as-prepared CNTs@$Fe_3O_4$ @RF nanocables can also be used as both reductant and template to synthesize the CNTs@$Fe_3O_4$@RF@Au nanocomposites from Au(III) salt within one step. As shown in Fig. 2(c-d), there are many satellite-like Au nanoparticles coated on the RF surface, and the size of Au nanoparticles lies in the range of 20-

150 nm. Because the redox reaction occurred to the solid-liquid interface, so no individual nanoparticles were found in the solution, indicating that the reduction of the noble metal nanoparticles takes place completely. The TEM image with higher resolution (Fig. 2d) shows that small Au aggregates (ca.150 nm) are dispersed in between the well-defined Au nanoparticles on the RF surface. This was also in accordance with our previous work[29]. In the following catalytic experiment, the synthesized CNTs@$Fe_3O_4$@RF@Au composites will be used for catalyzing the organic dye.

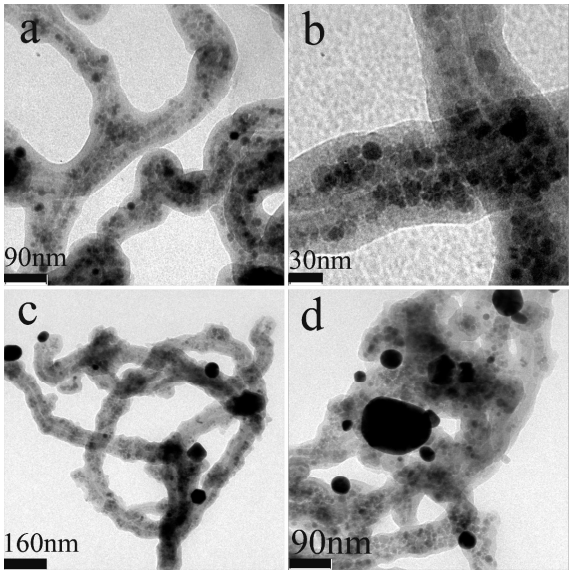


**Fig. 2** TEM images of (a-b) mesoporous carbon coated CNTs@$Fe_3O_4$ , and (c-d) CNTs@$Fe_3O_4$ @RF@Au

To further confirm the successful coating of RF resin on the surface of magnetic CNTs, the FTIR results are shown in Fig. 3a. The peak at 1616 $cm^{-1}$ represents the aromatic groups, and the peak at 1465 $cm^{-1}$ corresponds to the $–CH_2–$ groups, of which are expected for the coating of RF resin on the CNTs@$Fe_3O_4$. The other two absorption peaks at 2854 and 2900 $cm^{-1}$ are assigned to the $–CH_2$ group from CTAB. This suggests that the CTAB has been successfully encapsulated into the CNTs@$Fe_3O_4$ @RF. After the removal of CTAB by carbonization at 500°C, the intensity of the absorption peaks at 2854 and 2900 $cm^{-1}$ are greatly lessened, confirming that most of the CTAB was successfully removed (Fig. 3b).

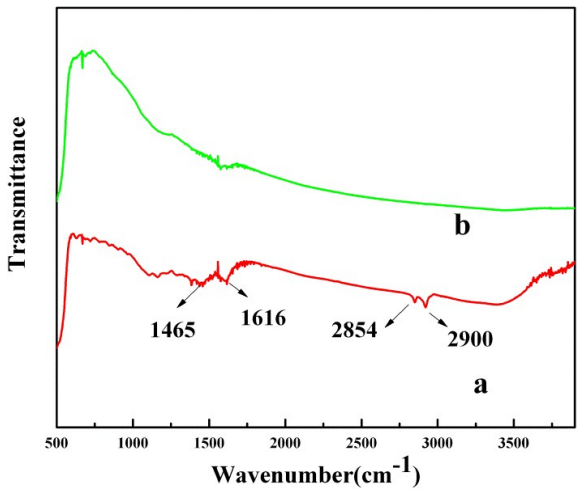


**Fig. 3** FT-IR spectra of (a) CNTs@$Fe_3O_4$ @RF, and (b) CNTs@$Fe_3O_4$ @C

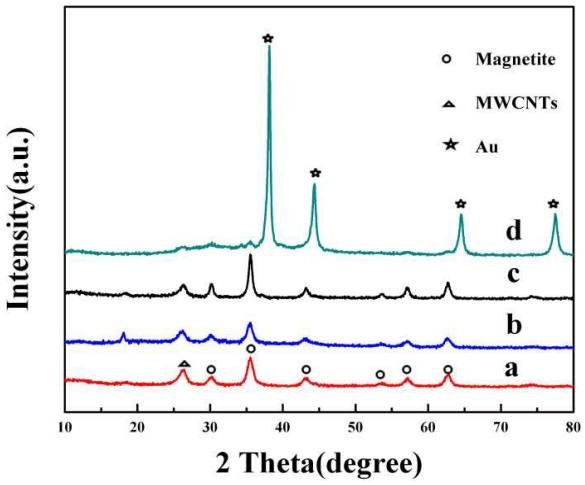


**Fig. 4** XRD diffraction patterns of (a) the as-prepared CNTs@$Fe_3O_4$ ,(b) CNTs@$Fe_3O_4$ @RF, (c) CNTs@$Fe_3O_4$ @C, and (d) CNTs@$Fe_3O_4$ @RF@Au NPs.

The crystalline structures of products at each step were characterized by XRD, which are shown in Fig. 4. According to Fig. 4a, the diffraction peaks of as received CNTs/$Fe_3O_4$ at 30.00º, 35.48º, 43.14º, 53.44º, 57.04º, and 62.58º were observed, which match well with the (220), (311), (400), (422), (511), and (440) planes of the standard cubic spinel crystal structure of bulk magnetite. The other two peaks at 25.98° and 42.78° are assigned to (002) and (100) planes of the MWCNTs, respectively[30].. The broadening of the diffraction peak indicates that the obtained magnetite crystallites are significantly small. As calculated by Scherrer's formula, the average crystallite size of the magnetite crystals was about 8 nm. The XRD pattern of CNTs@$Fe_3O_4$ @RF shows the similar peaks comparing

with the pristine CNTs@$Fe_3O_4$ particles (Fig. 4b), revealing that the as-prepared core–shell composites consist of the CNTs@$Fe_3O_4$ component. The major peaks of CNTs/$Fe_3O_4$@C composites (Fig. 4c) are similar to the pristine CNTs@$Fe_3O_4$ composites, except the appearing a broad diffraction peak at 2θ = 15-20° due to the amorphous carbon. Moreover, the peak intensity of $Fe_3O_4$ from the CNTs/$Fe_3O_4$@C composite was increased after calcination at high temperature, and the average crystallite size of the magnetite crystals was about 15 nm by Scherrer's formula, which indicated that the treatment on high temperature tend to sinter the $Fe_3O_4$ nanoparticles within the carbon shell. This will be further discussed in the following VSM experiments. The CNTs@$Fe_3O_4$@RF@Au composite shows four new peaks at 38°, 43°, 65° and 78°, which matches exactly with the Bragg reflections from (111), (200), (200) , and (311) planes of Au (JCPDS card No. 04-0784), suggesting the existence of Au NPs in the CNTs@$Fe_3O_4$@RF@Au composites (Fig. 4d).

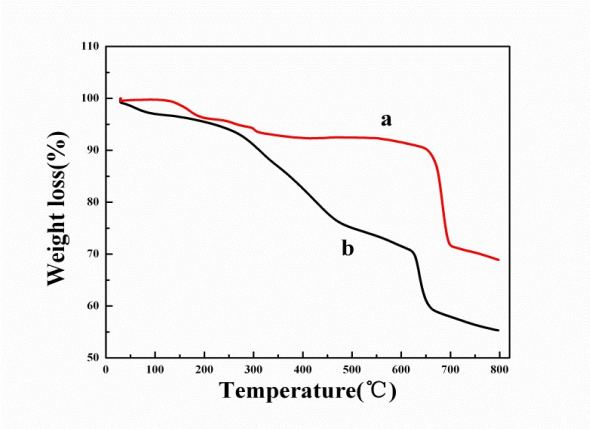


**Fig. 5** TGA of (a) CNTs@$Fe_3O_4$ , (b) CNTs@$Fe_3O_4$ @RF

The magnetic CNTs composites were analyzed by thermogravinetry analysis (TGA) upon heating in a nitrogen atmosphere. As shown in Fig. 5, both of the CNTs/$Fe_3O_4$ and CNTs@$Fe_3O_4$@RF composites show two degradation steps. The CNTs@$Fe_3O_4$ starts to lose weight at around 150 °C in a slow rate with 7 % weight loss till 300 °C, while turns into a rapid rate from 700 °C. The core–shell CNTs@$Fe_3O_4$@RF (Fig. 5b) show the first decomposition temperature starts early at 100 °C with a weight loss of about 35% till 650 °C, the decomposition of which is further more than the CNTs@$Fe_3O_4$, this was ascribed to the decomposition of CTAB and RF layer.

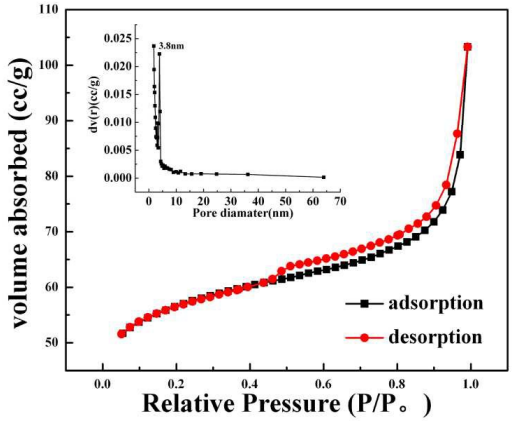


**Fig. 6** $N_2$ adsorption–desorption isotherms of CNTs@$Fe_3O_4$ @C.

Inset: pore size distributions.

The surface area and pore size distribution of CNTs@$Fe_3O_4$ @RF and CNTs@$Fe_3O_4$@C composites are tested by nitrogen adsorption–desorption (Fig. S3, Fig. 6). The nitrogen adsorption–desorption isotherms of the CNTs@$Fe_3O_4$@C display type-IV curves with a capillary condensation step at a low relative pressure ($P/P_0$ = 0.2–0.4), suggesting the existence of uniform mesopores.The BET surface area of CNTs@$Fe_3O_4$ @C is calculated to be 178.31 $m^2g^{-1}$, while that of the CNTs@$Fe_3O_4$ @RF was 16.62 $m^2g^{-1}$. Such a high surface area is attributed to the porous carbon layer of the CNTs@$Fe_3O_4$@C. There is a sharp pore distribution with an average diameter of 3.8 nm obtained by the BJH method. The high surface area and porous structure are beneficial for adsorption.

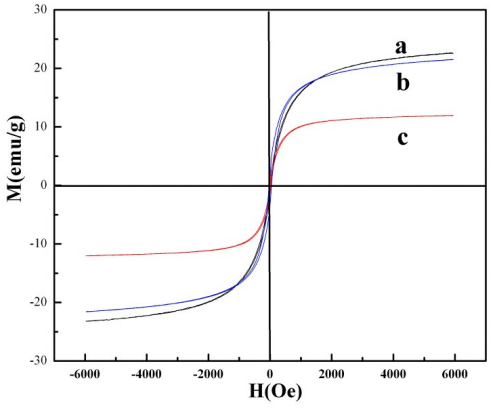


**Fig. 7** Hysteresis loops of (a) the magnetic CNTs@$Fe_3O_4$ , (b)

CNTs@$Fe_3O_4$ @C, and (c) CNTs@$Fe_3O_4$ @RF.

The super-paramagnetic behaviour of the magnetic composites was studied by vibrating sample in magnetometer at room temperature. The hysteresis loops of CNTs@$Fe_3O_4$, CNTs@$Fe_3O_4$ @C and CNTs@$Fe_3O_4$ @RF@Au are shown in Fig. 7. It can be seen that as-prepared magnetic particles (CNTs@$Fe_3O_4$ , CNTs@$Fe_3O_4$ @C) have fairly strong magnetization and the saturation

magnetization (MS) values are about 25 and 23 emu $g^{-1}$, respectively. The decrease in magnetic saturation of the CNTs@$Fe_3O_4$@RF@Au (around 8 emu $g^{-1}$) in comparison with CNTs@$Fe_3O_4$ may be attributed to the coated RF shell and Au on the surface of the CNTs@$Fe_3O_4$. It is worth mentioning that the CNTs@$Fe_3O_4$@C is ferromagnetic, which is due to that the magnetic nanoparticles decorated on the carbon nanotube tend to sinter and form bigger magnetic nanoparticles with the size above 10 nm at elevated temperatures. Notably, the sintering is entirely limited to within the shell confinement. And this is also in accordance with the XRD result. The relatively saturation magnetization value was conducive to accomplish efficient separation with an external magnet, which was an advantage for their application.

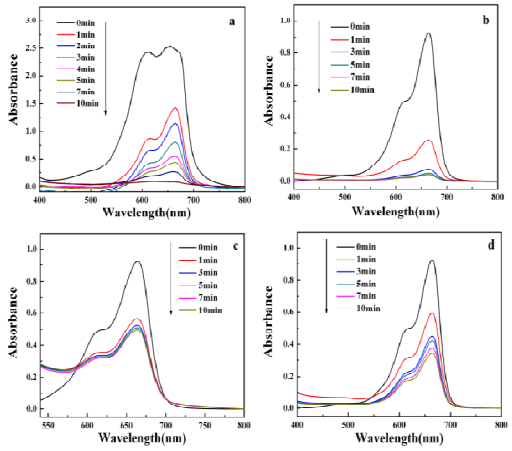


**Fig. 8** UV-Vis absorption spectra of MB(50 mg/L) by (a) CNTs/$Fe_3O_4$@RF@Au with $NaBH_4$, (b) UV-Vis absorption spectra of MB(5 mg/L) by CNTs/$Fe_3O_4$@C, (c) CNTs/$Fe_3O_4$, and (d) CNTs/$Fe_3O_4$@RF.

It has been long identified that Au NPs show excellent catalytic activity and selectivity on many catalytic reactions. Herein, the catalytic reduction of MB by $NaBH_4$ was used as a model reaction to investigate the catalytic performance of catalytic performance of CNTs@$Fe_3O_4$@RF@Au.This reaction can be monitored by the color bleaching of MB solution after the addition of the catalysts and an excess amount of $NaBH_4$, as indicated by the gradual decrease in the maximum absorbance values ($\lambda max$ = 665 nm) with time in the UV−vis spectra. To observe the whole catalysis process on the MB solution, the concentration of MB was set as 50 mg/L. When 2 mg CNTs@$Fe_3O_4$ @RF@Au composite nanoparticles were added into the mixture of $NaBH_4$ and MB, the dark blue mixture became transparent within 10 min. The changes are shown in Fig. 8a. Without the Au catalyst, the reduction of MB proceeded at a very slow speed with addition of $NaBH_4$, the color of the MB solution almost disappear after several days.[31] The catalytic results reveal that the as-synthesized CNTs@$Fe_3O_4$@RF@Au nanocatalyst shows a higher catalytic performance. The catalytic results reveal that the as-synthesized CNTs@$Fe_3O_4$@RF@Au nanocatalyst show higher catalytic performance, which may be partly caused by the effective contact between RF and Au nanocatalysts, while in this catalytic reaction for $Fe_3O_4$@$SiO_2$ nanocomposites, the relatively high concentration of $NaBH_4$ slowly etches the silica surfaces, which lead to the gradual detachment of Au nanoparticles from the support surface and dramatically reduced their catalytic activity[32]. Therefore, compared to the Au immobilized on $SiO_2$/$Fe_3O_4$ that has been studied, CNTs@$Fe_3O_4$ @RF@Au nanocatalyst exhibited much higher stability in various chemical and physical environments. After reaction, the CNTs@$Fe_3O_4$@RF@Au can be easily removed from the reaction solution by an external magnetic field.

Meanwhile, the as-prepared mesoporous CNTs@$Fe_3O_4$@C was used as absorbents in dyes treatment. Organic dyes have been considered as a primary toxic pollutant in water resources. In this study, in order to illustrate the high uptake capacity of the mesoporous CNTs@$Fe_3O_4$@C, the CNTs@$Fe_3O_4$ and CNTs@$Fe_3O_4$ @RF were used as the control. The methylene blue (MB), a typical organic dye, was chosen as testing organic pollutant. 5 mg of the as-prepared product as the sorbent was added into the MB solution with initial concentration of 5 mg $L^{-1}$. Absorption spectra of a solution of methylene blue in the presence of three kinds of materials at different time were monitored by UV-Vis spectrophotometer (Fig. 8(b,c,d)). The obvious colour change of the aqueous dye solution was observed. From the Fig. 8b, it can be observed that the adsorption rate was the blue mixture became light blue within 1 min at a high rate of speed. Then the adsorption rate become slowly, 10 min later, the solution is nearly transparent. We believe that the efficient removal is mainly attributed to its small pore size and high surface area of the structure of the mesoporous CNTs@$Fe_3O_4$@C. In contrast to CNTs@$Fe_3O_4$ and CNTs@$Fe_3O_4$ @RF, they showed the smaller adsorption capacity (Fig. 8(c,d)). The adsorption ability of CNTs@$Fe_3O_4$ and CNTs@$Fe_3O_4$@RF may be attributed to the hydrogen bonding and electrostatic interaction between the MB and the surface of CNTs@$Fe_3O_4$ and CNTs@$Fe_3O_4$@RF. These demonstrated that the mesoporous CNTs@$Fe_3O_4$@C have much greater MB removal efficiency than that of the other two materials. After removal of the remaining MB by calcinations at 350ºC in air for 2 hours, the mesoporous CNTs@$Fe_3O_4$@C can be activated for adsorption again.

## Conclusions and Out look

In summary, we have demonstrated a simple, reproducible method of preparing core-shell CNTs@$Fe_3O_4$@RF composites. On the basis of the CNTs@$Fe_3O_4$ nanocables, RF-resin shell can be directly coated on the nanocables surface to form the CNTs@$Fe_3O_4$@RF nanocables with well-defined core-shell nanostructure. By means of the interfacial reduction between RF shell and $HAuCl_4$ solution, plentiful Au nanoparticles are well decorated onto the surface of CNTs@$Fe_3O_4$@RF carriers to form the CNTs@$Fe_3O_4$@RF@Au nanocables. These Au-immobilized composites exhibit excellent catalytic properties as the demonstration on the reduction of MB with $NaBH_4$. Meanwhile, the mesoporous carbon coated CNTs@$Fe_3O_4$ was also obtained by calcination in nitrogen atmosphere. More importantly, these results offer a powerful platform to construct other multicomponent composite nanocables, which are likely found many potential catalytic and biomedical applications derived from their rational combination of magnetic

properties with surface plasmon resonance, protein separation, or catalysis.

**ACKNOWLEDGMENT**

The authors are grateful to the financial support by the National Science Foundation of China (No 21305086). The Natural Science Foundation of Shanghai City (13ZR141830), Research Innovation Program of Shanghai Municipal Education Commission (14YZ138), the Special Scientific Foundation for Outstanding Young Teachers in Shanghai Higher Education Institutions (ZZGJD13016 ), and Start-up Funding of Shanghai University of Engineering Science.

**Notes and references**

College of Chemistry and Chemical Engineering, Shanghai University of Engineering Science, Shanghai 201620, China. E-mail: zhangmin@sues.edu.cn; xujingli@sues.edu.cn.

## References

1. S. Guo, S. Dong and E. Wang, *Advanced Materials*, 2010, **22**, 1269-+.
2. P. Singh, J. Kumar, F. M. Toma, J. Raya, M. Prato, B. Fabre, S. Verma and A. Bianco, *Journal of the American Chemical Society*, 2009, **131**, 13555-13562.
3. D. R. Kauffman and A. Star, *Angewandte Chemie International Edition*, 2008, **47**, 6550-6570.
4. G. G. Wildgoose, C. E. Banks and R. G. Compton, *Small*, 2006, **2**, 182-193.
5. J. H. Choi, F. T. Nguyen, P. W. Barone, D. A. Heller, A. E. Moll, D. Patel, S. A. Boppart and M. S. Strano, *Nano Letters*, 2007, **7**, 861-867.
6. C. Gao, W. Li, H. Morimoto, Y. Nagaoka and T. Maekawa, *The Journal of Physical Chemistry B*, 2006, **110**, 7213-7220.
7. D. Yang, F. Yang, J. Hu, J. Long, C. Wang, D. Fu and Q. Ni, *Chemical Communications*, 2009, DOI: 10.1039/B908012K, 4447-4449.
8. C. L. Chen, X. K. Wang and M. Nagatsu, *Environmental Science & Technology*, 2009, **43**, 2362-2367.
9. X. Zhao, C. Johnston and P. S. Grant, *Journal of Materials Chemistry*, 2009, **19**, 8755-8760.
10. H. Dong, Y. C. Chen and C. Feldmann, *Green Chemistry*, 2015, **17**, 4107-4132.
11. Z. Sun, Z. Liu, Y. Wang, B. Han, J. Du and J. Zhang, *Journal of Materials Chemistry*, 2005, **15**, 4497-4501.
12. Q. Liu, Z.-G. Chen, B. Liu, W. Ren, F. Li, H. Cong and H.-M. Cheng, *Carbon*, 2008, **46**, 1892-1902.
13. J. Wan, W. Cai, J. Feng, X. Meng and E. Liu, *Journal of Materials Chemistry*, 2007, **17**, 1188-1192.
14. N. Li, Q. Zhang, J. Liu, J. Joo, A. Lee, Y. Gan and Y. Yin, *Chemical Communications*, 2013, **49**, 5135-5137.
15. B. Guan, X. Wang, Y. Xiao, Y. Liu and Q. Huo, *Nanoscale*, 2013, **5**, 2469-2475.
16. H.-W. Liang, J.-W. Liu, H.-S. Qian and S.-H. Yu, *Accounts of Chemical Research*, 2013, **46**, 1450-1461.
17. Y. Liu, K. Ai and L. Lu, *Chemical Reviews*, 2014, **114**, 5057-5115.
18. J. Liu, S. Z. Qiao, H. Liu, J. Chen, A. Orpe, D. Zhao and G. Q. Lu, *Angewandte Chemie International Edition*, 2011, **50**, 5947-5951.
19. A. B. Fuertes, P. Valle-Vigon and M. Sevilla, *Chemical Communications*, 2012, **48**, 6124-6126.
20. R. Liu, F. Qu, Y. Guo, N. Yao and R. D. Priestley, *Chemical Communications*, 2014, **50**, 478-480.
21. R. Liu, Y.-W. Yeh, V. H. Tam, F. Qu, N. Yao and R. D. Priestley, *Chemical Communications*, 2014, **50**, 9056-9059.
22. P. Yang , Q.-Z. Xu, S.-Y. Jin, Y. Zhao, Y. Lu, X.-W. Xu and S.-H. Yu, *Chemistry – A European Journal*, 2012, **18**, 1154-1160.
23. P. Yang, Y. Zhao, Y. Lu, Q.-Z. Xu, X.-W. Xu, L. Dong and S.-H. Yu, *ACS Nano*, 2011, **5**, 2147-2154.
24. Q. Zhang, X.-Z. Shu, J. M. Lucas, F. D. Toste, G. A. Somorjai and A. P. Alivisatos, *Nano Letters*, 2014, **14**, 379-383.
25. T. Yang, J. Liu, Y. Zheng, M. J. Monteiro and S. Z. Qiao, *Chemistry – A European Journal*, 2013, **19**, 6942-6945.
26. P. Yang, Q.-Z. Xu, S.-Y. Jin, Y. Lu, Y. Zhao and S.-H. Yu, *Chemistry – A European Journal*, 2012, **18**, 9294-9299.
27. S.-R. Guo, J.-Y. Gong, P. Jiang, M. Wu, Y. Lu and S.-H. Yu, *Advanced Functional Materials*, 2008, **18**, 872-879.
28. P. Yang, Y. Xu, L. Chen, X. Wang and Q. Zhang, *Langmuir*, 2015, **31**, 11701-11708.
29. M. Zhang, P. Xia, L. Wang, J. Zheng, Y. Wang, J. Xu and L. Wang, *Rsc Advances*, 2014, **4**, 44423-44426.
30. B. Fei, B. Qian, Z. Yang, R. Wang, W. C. Liu, C. L. Mak and J. H. Xin, *Carbon*, 2008, **46**, 1795-1797.
31. T. Yao, C. Wang, J. Wu, Q. Lin, H. Lv, K. Zhang, K. Yu and B. Yang, *J. Colloid Interface Sci.*, 2009, **338**, 573-577.
32. S. Xuan, Y.-X. J. Wang, J. C. Yu and K. C.-F. Leung, *Langmuir*, 2009, **25**, 11835-11843.

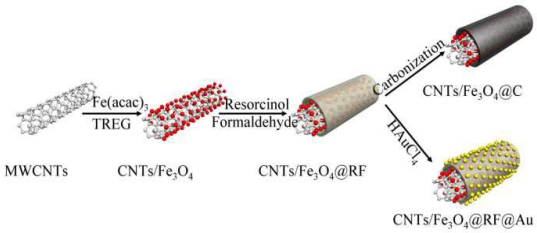


The $CNTs/Fe_3O_4@RF@Au$ and $CNTs/Fe_3O_4@C$ composites were achieved via the reduction of $Au^{3+}$ by the $CNTs/Fe_3O_4@RF$ composite itself or calcinations in inert atmosphere respectively.